Rock Mechanics and Rock Engineering (2020) 53:2493–2503
https://doi.org/10.1007/s00603-020-02049-8

TECHNICAL NOTE

Numerical Modelling of Fully Grouted Rockbolts Subjected to Shear Load

Wen Nie[1,2] · Wei Guo[3] · Shuqi Ma[4] · Zhiye Zhao[5]

Received: 7 May 2019 / Accepted: 7 January 2020 / Published online: 25 January 2020

Keywords Rockbolt · Rock joint · Bond stress · Shear · DDA

List of Symbols

A_b	Cross-sectional area of rockbolt
D_b	Diameter of rockbolt
E_b	Elastic modulus of rockbolt
E_r	Young's modulus of rock
F_s	Shear load at the joint of the rockbolt element
$F_{s,max}$	Maximum shear load at the joint of the rockbolt element
$F_{s,y}$	Shear load of rockbolt element at yielding
I_b	Inertia of rockbolt cross section
k_0	Bond stiffness of rockbolt element at the rockbolt/rock interface
K_s	Shear stiffness of rockbolt element
l_e	Hinge length of rockbolt element at joint
N	Axial load of rockbolt element
N_y	Yielded axial load of rockbolt element
N_f	Ultimate axial load of rockbolt element
U_b	Axial movement of rockbolt
U_r	Axial displacement of rockbolt
U_s	Shear displacement of rockbolt at joint
α_o	Deflection angle of rockbolt element crossing joint
β	Incline angle of rockbolt element at joint
γ_r	Unit weight of rock
τ	Bond stress at the rockbolt/rock interface
κ	Concentration coefficient of the shear stress distribution at the cross section

✉ Wei Guo
guow@tju.edu.cn

Wen Nie
wnie001@e.ntu.edu.sg

Shuqi Ma
shuqima.ma@gmail.com

Zhiye Zhao
CZZhao@ntu.edu.sg

[1] School of Civil and Transportation Engineering, Hebei University of Technology, Tianjin 300401, China

[2] State Key Laboratory for GeoMechnics and Deep Underground Engineering, China University of Mining and Technology (Beijing), Beijing 10083, China

[3] School of Civil Engineering, Tianjin University, 135 Yaguan Road, Jinnan District, Tianjin 300350, China

[4] Civil and Environmental Engineering, Colorado School of Mines, Golden, CO 80401, USA

[5] School of Civil and Environmental Engineering, Nanyang Technological University, 50 Nanyang Ave, Singapore 639798, Singapore

1 Introduction

Rockbolts are often installed into the rock masses as a reinforcement structure to restrain the rock deformation at the excavation surface in underground excavation projects. When the rock moves towards the excavation surface, the rockbolt elongates, resulting in tension in the rockbolt and compression in the surrounding rock mass (Bobet and Einstein 2011). The most commonly used rockbolt is the fully grouted rockbolt as it has a reliable anchoring system and high bearing capacity (Li and Stillborg 1999). The mortar and resin are often used as the grouting agent and filled in the annulus between the rockbolt and the borehole wall. The load transferring capacity of the fully grouted rockbolt is, therefore, heavily dependent on the bond strengths at the interfaces between the rockbolt and the grout and between the grout and the rock (Hyett et al. 1992; Ma et al. 2014; Nie et al. 2019).

The performances of a fully grouted rockbolt under different loading conditions have been investigated by several laboratory tests (Chen and Li 2015; Grasselli 2005; Jalalifar and Aziz 2010). It has been found in these tests that the failure of a fully grouted rockbolt usually occurred within the region of the discontinuities. Field monitoring results

show that the shear strength of the fully grouted rockbolt is equally important to its tensile strength (Li 2010). Different analytical solutions have been proposed in the literatures to determine the failure in the local region of the discontinuities (Ferrero 1995; Li et al. 2015; Ma et al. 2018; Pellet and Egger 1996). To evaluate the influence of the fully grouted rockbolt on the shear resistance of a single joint, a simplified analytical model has been developed based on beam theory (Li et al. 2015). Numerical models for rockbolts have also been developed to investigate the reinforcement effects of rockbolt on the rock mass (Bahrani and Hadjigeorgiou 2017; Li et al. 2016; Nemcik et al. 2014; Qian and Zhou 2018).

The numerical rockbolt models have the advantages in accommodating the rockbolt models into the rock structures. The representation of rock movement using numerical modelling might be required in some cases to represent the block deformation (Karampinos et al. 2015). The discontinuous deformation analysis (DDA) method developed and programmed by Shi (1988) is capable to simulate the static and dynamic behaviors of discrete blocky systems based on block kinematics. To simulate the interaction between rock and rockbolt, a rockbolt model has been developed and integrated into the DDA program by Nie et al. (2014a, b). However, the failure propagation in the rockbolt model, especially the plastic hinge formation near the rock joint and the shear failure of rockbolt material were not included in the rockbolt model.

In this study, the rockbolt model proposed by Nie et al. (2014a, b) is modified to simulate the failure mechanism of the fully grouted rockbolt installed in the jointed rock mass subjecting to the combined tension and shear loads. The mechanical behavior of the fully grouted rockbolt at rock joints is analyzed based on beam theory and integrated into the DDA code. The numerical results are compared with those from laboratory single shear tests and double shear tests. The advantages and limitations of the modified fully grouted rockbolt model are also discussed.

2 Rockbolt Modelling in DDA

2.1 Governing Equations

The DDA method adopts an incremental solution procedure. The dynamic equations of the block system are solved at each time step, while the incremental changes in energy are determined at the same time as the block system attempts to reach equilibrium (Shi 1988). The basic framework of the multi-time step calculations in DDA contains the following three parts, i.e., the input, the multi-time step procedure and the output, as shown in Fig. 1. The properties of blocks and joints are defined at the beginning of the calculation. The maximum displacement ratio and the upper limit of time interval are used to determine the incremental time step and control the open–close iteration. To solve the governing equations, the successive over relaxation (SOR) method is used. More details of the calculation procedure can be found in Shi (1988).

In DDA, the deformation of a single block has six basic variables in the first-order approximation, as shown in Fig. 2. In each time step, the displacements of a point (x, y) in a block are represented as

$$\{u_i\} = [T_i]\{D_i\}, \tag{1}$$

in which $[T_i]$ is expressed as follows,

$$[T_i] = \begin{bmatrix} 1 & 0 & -(y-y_0) & (x-x_0) & 0 & (y-y_0)/2 \\ 0 & 1 & (x-x_0) & 0 & (y-y_0) & (x-x_0)/2 \end{bmatrix}, \tag{2}$$

where $\{D_i\} = (u_0, v_0, r_0, \varepsilon_x, \varepsilon_y, \gamma_{xy})^{\mathrm{T}}$, i is the block ID; u_0 and v_0 are the rigid body translation at a specific point (x_0, y_0) within the block i; r_0 is the rotation angle of the block i with respect to (x_0, y_0); ε_x and ε_y are the normal strains in the x and y directions, respectively, and γ_{xy} is the shear strain.

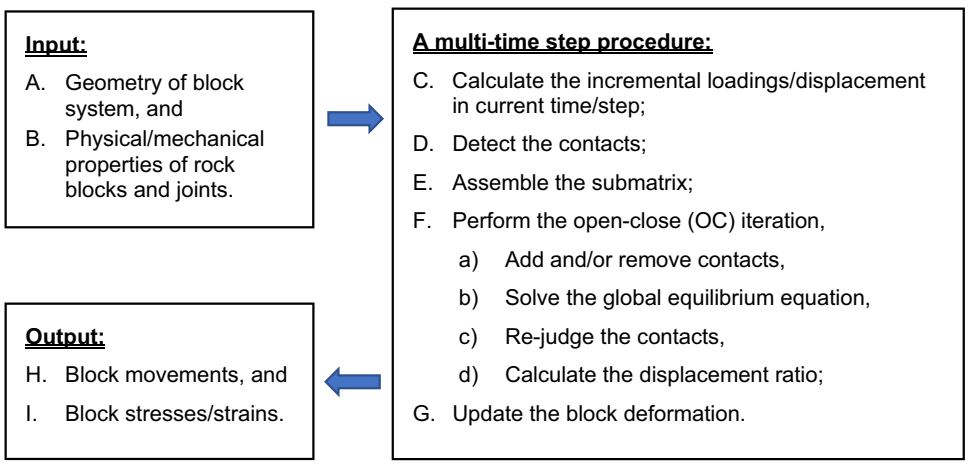

Fig. 1 Framework of the multi-time step calculation in DDA (Nie 2019)

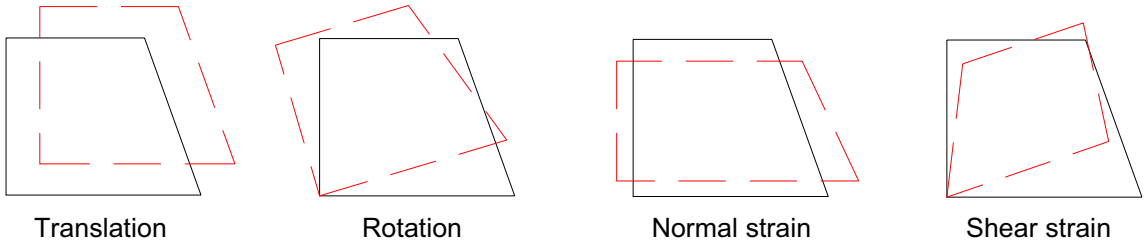

Fig. 2 Displacement variables of a single block in the first-order approximation in DDA (Shi 1988; Hatzor et al. 2017)

For a blocky system containing n blocks, the global equilibrium equation in matrix form is shown as follows

$$[K_{ij}]\{D_i\} = \{F_i\}. \tag{3}$$

The matrix $[K_{ij}]$ $(i, j = 1, 2, \ldots, n)$ is given as follows

$$[K_{ij}] = \frac{\partial^2 \prod}{\partial d_{ri} \partial d_{sj}} (r, s = 1, 2, \ldots, 6), \tag{4}$$

where Π is the total potential energy of the whole system; d_{ri} is the displacement vector; for $(i \neq j)$, $[K_{ij}]$ is a 6×6 submatrix to represent the contacts between blocks i and j $(i, j = 1, \ldots, n)$, and for $(i = j)$, $[K_{ij}]$ is the local stiffness matrix.

The matrix $\{F_i\}$ $(i = 1, 2, \ldots, n)$ is a 6×1 sub matrix representing the loading on block i distributed to the six deformation variables, and it is given by

$$\{F_i\} = -\left(\frac{\partial \prod}{\partial d_{ri}}\right)\Bigg|_{d_{ri}=0} (r = 1, 2, \ldots, 6). \tag{5}$$

More derivation details of matrix $[K_{ij}]$ and $\{F_i\}$ could be found in Hatzor et al. (2017). To simulate the reinforcement provided by rockbolts, the sub matrix of point loads has to be considered. Take a point load (F_x, F_y) acting on a point (x, y) for example, its contribution to the submatrix $\{F_i\}$ is given as

$$[T]^{\mathrm{T}} \begin{bmatrix} F_x \\ F_y \end{bmatrix} \rightarrow \{F_i\}. \tag{6}$$

2.2 Rockbolt Model Under Pure Tension

To better model the interaction between the rock and the rockbolt, a rockbolt is separated into a few segments by the block boundaries. The positive direction of the rockbolt is defined as the direction from its embedded free end to the other end, where the faceplate might be attached. An example of a fully grouted rockbolt installed through rock blocks A, B and C is shown in Fig. 3. The rockbolt is divided into three segments and each segment contains several rockbolt elements. The suggested length of one element for a fully grouted rockbolt is less than 0.1 m (Blanco Martín et al. 2013). Two nodes at the same location, one on the rockbolt (rockbolt node) and the other one on the rock block (rock node), are isolated to determine the relative displacement between them. Once the rock block deforms, the relative movements between the rock nodes and the rockbolt nodes are used to calculate the slip displacement. Based on the calculated relative movements between the rockbolt and the rock, the change in bond stress $\Delta\tau_i$ along rockbolt could be calculated according to the bond-slip model (Farmer 1975)

$$\Delta\tau_i = k_0\left(U_{\mathrm{r}} - U_{\mathrm{b}}\right), \tag{7}$$

where k_0 is the bond stiffness at the rockbolt and rock interface; U_{r} and U_{b} are the movements of rock and rockbolt, respectively, and $\Delta\tau_i$ is the change of bond stress on the interface of the ith rockbolt element and rock.

The force equilibrium at a rockbolt element gives the change of axial stress as

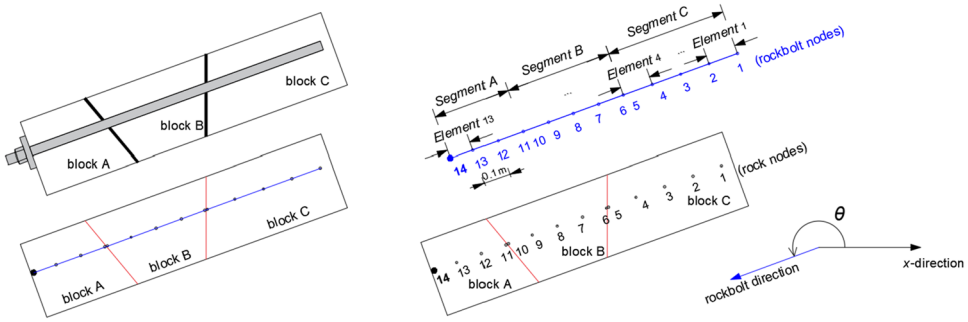

Fig. 3 Element divisions of a fully grouted rockbolt installed through several rock blocks

$$\Delta\sigma_i = \frac{\Delta N}{A_b} = \frac{\Delta\tau_i l_i}{A_b}\pi D_b, \tag{8}$$

where $\Delta\sigma_i$ is the variation of the axial stress in the ith rockbolt element; l_i is the length of the ith rockbolt element; A_b is the cross-sectional area of rockbolt, and D_b is the diameter of rockbolt.

The rockbolt is assumed as a bilinear strain-hardening material with elastic modulus of E_b and strain-hardening modulus of E_T (see Fig. 4a). The tri-linear bond-slip model is used to simulate the bonding behaviour between the rock mass and the fully grouted rockbolt (Ma et al. 2017; Nie et al. 2019). As shown in Fig. 4b, the tri-linear bond-slip model separates the bond stress versus slip displacement curve into three simplified linear sections with three different bond stiffness, i.e., k_1, k_2 and k_3 are the bond stiffness for the ascending section, the softening section and the residual section, respectively. For a given rockbolt with a total node number of n and a total element number of $(n-1)$, by assuming the displacement within one element varies quadratically, the mathematical algorithm of the rockbolt model can be obtained by combining Eqs. (7) and (8), so we have

$$\frac{A_b E_b}{l_{i-1}}\left(U_b^i - U_b^{i-1}\right) + \frac{A_b E_b}{l_i}\left(U_b^i - U_b^{i+1}\right) = k\left(\frac{l_i + l_{i-1}}{2}\right)\left(U_r^i - U_b^i\right), \tag{9}$$

where $k = k_0\pi D_b$ and E_b is the elastic modulus of rockbolt material.

For the rockbolt node located on the faceplate, the displacements for the rock node and the rockbolt node are the same, i.e., $U_r^n = U_b^n$, which gives the force acting on the faceplate ΔP_n as

$$\Delta P_n = \frac{A_b E_b}{l_{n-1}}\left(U_r^{n-1} - U_r^n\right). \tag{10}$$

The increment of restraint force provided by the rockbolt at the rockbolt node i ($i = 1, \ldots, n-1$), ΔP_i could be calculated as

$$\Delta P_i = k l_i\left(U_r^i - U_{bx}^i\right). \tag{11}$$

By defining the angle between the rockbolt direction and x-axis as θ (see Fig. 3), the point loads to the rock block induced by the restraints of rockbolt at a time step could be calculated as

$$\begin{bmatrix} F_x \\ F_y \end{bmatrix} = -\Delta P_i \begin{bmatrix} \cos\theta \\ \sin\theta \end{bmatrix}, \tag{12}$$

where F_x and F_y are the point loads at the horizontal and vertical directions, respectively.

Because the yield criteria which is based on nominal strain of the rockbolt could not consider the shear stress components, the reaction shear force from rockbolt to rock block due to joint dislocation are not included. It is necessary to develop a new numerical model to consider the shear loads onto the rockbolts when they are installed through rock joints.

2.3 Rockbolt Model Considering Tension and Shear

When a fully grouted rockbolt is subjected to shear load at a rock joint, the rockbolt may deflect. The deformation of the rockbolt exhibits two singular points symmetric with respect to the shear plane (Pellet and Egger 1996), such as the points A and C in Fig. 5a. The reaction force in the host material is mobilized at the beginning of loading process. The shear component of reaction force F_s is roughly proportional to the shape of the deflection of section AC in the elastic stage. Once the complete plasticization is reached, F_s is constant in the plastic stage. In DDA simulation, one potential plastic hinge might form at each side of the joint plane, such as AO and OC in Fig. 5b. The remained length of the rockbolt element through the rock joint is $2l_e$ where l_e is the hinge length of the rockbolt. If there is no experimental data supported, the hinge length l_e is often taken as 1.0–2.0 D_b, where D_b is the diameter of the rockbolt (Gerdeen et al. 1981; Grasselli 2005; Jalalifar

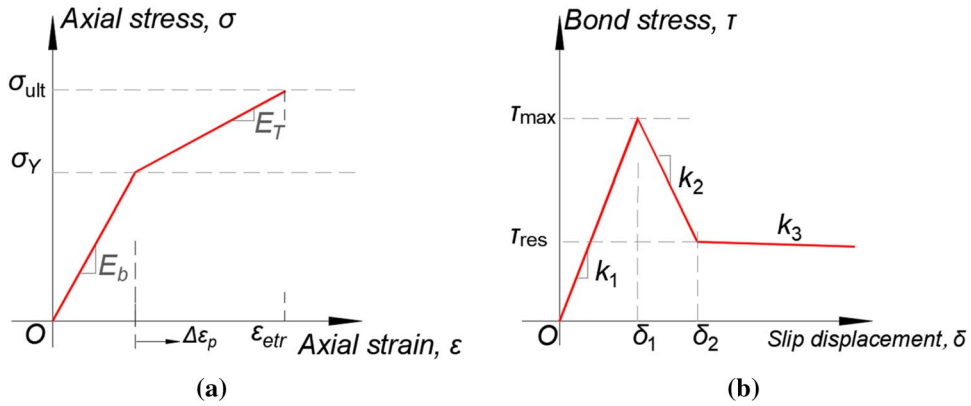

Fig. 4 Mechanical behaviours of **a** fully grouted rockbolt and **b** interface between rock and rockbolt

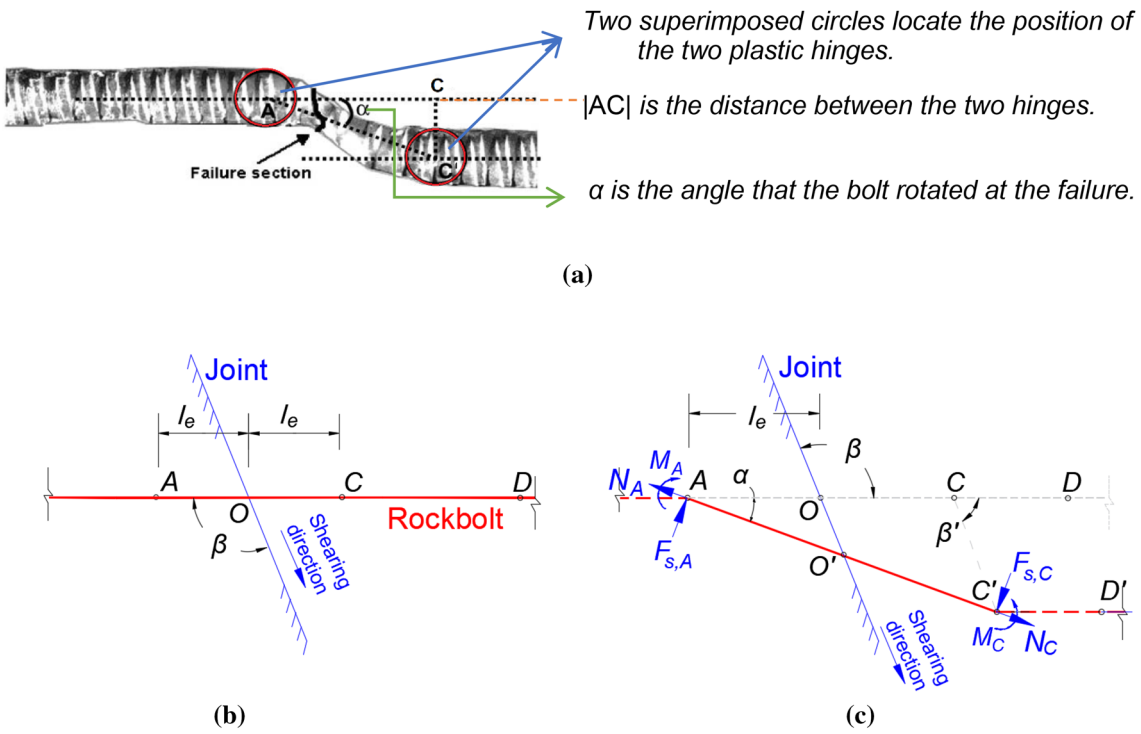

Fig. 5 Rockbolt element subjected to a shear movement **a** shape of a 20 mm diameter rockbolt extracted at the end of a shear test (modified after Grasselli 2005), **b** positions of rockbolt before shearing, and **c** positions and loads generated in the rockbolt element after shearing

and Aziz 2010). The directions of the generated axial load N, shear load F_s and bending moment M at two ends of the element of the fully grouted rockbolt are shown in Fig. 5c.

An example of a rockbolt crossing a rock joint with the direction angle of θ, and the incline angle between rock joint and rockbolt of β is presented in Fig. 6a. The analytical solution to consider the effects of combined tension and shear loads onto the yield performance of rockbolt is given by Li et al. (2015) and shown as

$$\begin{bmatrix} \frac{l_e}{E_b A_b} & 0 & 0 \\ 0 & \frac{l_e^3}{3E_b I_b + \frac{\kappa l_e}{G_b A_b}} & \frac{l_e^2}{2E_b I_b} \\ 0 & \frac{l_e^2}{2E_b I_b} & \frac{l_e}{E_b A_b} \end{bmatrix} \begin{Bmatrix} N_o \\ F_{so} \\ M_o \end{Bmatrix} - \begin{Bmatrix} 0 \\ \frac{q_0 l_e^4}{360 E_b I_b} + \frac{\kappa q_0 l_e^2}{12 G_b A_b} \\ \frac{q_0 l_e^3}{60 E_b I_b} \end{Bmatrix} = \begin{Bmatrix} U_b \\ U_s \\ \alpha_0 \end{Bmatrix}, \tag{13}$$

where N_o is the axial load; F_{so} is the shear load at the joint of rockbolt element; M_o is the bending moment; G_b is the shear modulus of the rockbolt; I_b is the inertia of rockbolt cross section; κ is a concentration coefficient of the shear stress distribution at the cross section which is equal to 4/3 of the solid cross section; U_b is the axial movement of rockbolt; U_s is the shear displacement of rockbolt at joint, and α_o is the deflection angle of rockbolt element crossing joint.

For a symmetrical homogenous beam element with a very small diameter, the bending moment M_o could be neglected. The force equilibrium at the rockbolt gives the axial load N_o and shear load F_{so} at a point O as

$$N_o = \frac{E_b A_b}{l_e} U_b, \tag{14}$$

$$F_{so} = \frac{240\kappa G_b A_b E_b^2 I_b^2 - 40 G_b^2 A_b^2 E_b I_b l_e^2}{\left(6E_b I_b \kappa l_e - G_b A_b l_e^3\right)\left(13 G_b A_b l_e^3 + 30\kappa E_b I_b\right)} U_s. \tag{15}$$

The rockbolt deformations along its shear and axial directions are correlated and shown as (Li et al. 2015)

$$U_s = \frac{\sin\beta}{\cos\left(\beta + \alpha_o\right)} U_b \approx \frac{\sin\beta}{\cos\beta - \alpha_o \sin\beta} U_b. \tag{16}$$

As shown in Fig. 6a, the force equilibrium on point A gives the expressions of axial load N_A, shear load F_{sA} and bending moment M_A as

$$N_A = \frac{E_b A_b}{l_e} U_b, \tag{17}$$

$$F_{sA} = K_s U_s, \tag{18}$$

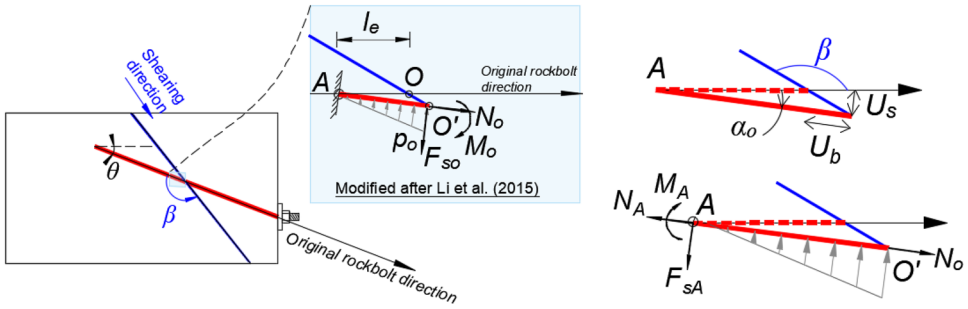

(a)

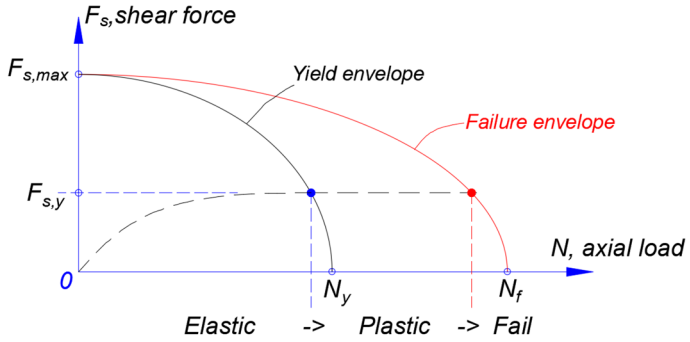

(b)

Fig. 6 Mechanical models of the rockbolt element **a** a free body diagram of rockbolt installed crossing a joint, and **b** loading state judgement using shear force versus axial load curve

$$M_{\mathrm{A}} = F_{\mathrm{sA}} l_{\mathrm{e}}, \tag{19}$$

where K_{s} is the shear stiffness of the rockbolt element with its expression shown as

$$K_{\mathrm{s}} = \frac{240\kappa G_{\mathrm{b}} A_{\mathrm{b}} E_{\mathrm{b}}^2 I_{\mathrm{b}}^2 - 40 G_{\mathrm{b}}^2 A_{\mathrm{b}}^2 E_{\mathrm{b}} I_{\mathrm{b}} l_{\mathrm{e}}^2}{\left(6E_{\mathrm{b}} I_{\mathrm{b}} \kappa l_{\mathrm{e}} - G_{\mathrm{b}} A_{\mathrm{b}} l_{\mathrm{e}}^3\right)\left(13 G_{\mathrm{b}} A_{\mathrm{b}} l_{\mathrm{e}}^3 + 30\kappa E_{\mathrm{b}} I_{\mathrm{b}}\right)}. \tag{20}$$

Based on Eqs. (17)–(19), the increase of axial load ΔN_{A}, shear load ΔF_{sA} and bending moment ΔM_{A} of the rockbolt element at a time step, respectively, can be derived as

$$\Delta N_{\mathrm{A}} = \frac{E_{\mathrm{b}} A_{\mathrm{b}}}{l_{\mathrm{e}}} \Delta U_{\mathrm{b}}, \tag{21}$$

$$\Delta F_{\mathrm{sA}} = K_{\mathrm{s}} \Delta U_{\mathrm{s}}, \tag{22}$$

$$\Delta M_{\mathrm{A}} = \Delta F_{\mathrm{sA}} l_{\mathrm{e}}. \tag{23}$$

The increase of axial stress $\Delta\sigma_{\mathrm{M}}$ induced by the bending moment acting at point A of the rockbolt element is given as

$$\Delta\sigma_{\mathrm{M}} = \frac{\Delta M_{\mathrm{A}} D_{\mathrm{b}}}{2I_{\mathrm{b}}}. \tag{24}$$

Combining Eqs. (8) and (24) gives the increase of normal stress of rockbolt element as

$$\Delta\sigma_{\mathrm{M}} = \frac{\Delta N_{\mathrm{A}}}{A_{\mathrm{b}}} + \frac{\Delta M_{\mathrm{A}} D_{\mathrm{b}}}{2I_{\mathrm{b}}}. \tag{25}$$

For short span beams carrying large concentrated loads, the reduction from shear is significant (Ssj 1996). The Von Mises yield criterion is usually used to describe the short span beam and shown as

$$\left(\frac{\sigma_{\mathrm{A}} A_{\mathrm{b}}}{N_{\mathrm{y}}}\right)^2 + \left(\frac{F_{\mathrm{sA}}}{F_{\mathrm{s,max}}}\right)^2 = 1, \tag{26}$$

where N_{y} is the yield axial load of rockbolt element under pure tension and $F_{\mathrm{s,max}} = N_{\mathrm{y}} \Big/ \sqrt{3}$.

By assuming the shear stress and moment of rockbolt element do not increase with respect to the increase of shear displacement once the rockbolt element is at yielded stage, the axial stress versus axial strain curve is still linear with its strain-hardening modulus of E_{T}. Equation (26) can be simplified as

$$\left(\frac{\sigma_{\mathrm{A}} A_{\mathrm{b}}}{N_{\mathrm{f}}}\right)^2 + \left(\frac{F_{\mathrm{s,y}}}{F_{\mathrm{s,max}}}\right)^2 = 1, \tag{27}$$

where $F_{\mathrm{s,y}}$ is the shear load of a rockbolt element at yielding, and N_{f} is the ultimate axial load of a rockbolt element under pure tension.

Under the combined tension and shear loads, the point loads to the rock blocks induced by rockbolt restraints at a time step could be calculated as

$$\begin{bmatrix} F_x \\ F_y \end{bmatrix} = \left(-\Delta P_i\right)\begin{bmatrix} \cos\theta \\ \sin\theta \end{bmatrix} + \left(-\Delta F_{\mathrm{sA}}\right)\begin{bmatrix} \sin\theta \\ \cos\theta \end{bmatrix}. \tag{28}$$

The point load matrix as shown in Eq. (28) will be added to the submatrix of $\{F_i\}$ in Eq. (6) in the multi-step procedure to simulate the reinforcements of rockbolt onto the rock blocks. The procedure for coding the proposed numerical rockbolt model into DDA program is shown in Fig. 7. The procedure only involves the geometry and the loading parts. The geometry part will add at the beginning of the multi-time step procedure (before C) in the basic framework of DDA, as shown in Fig. 1. The rockbolt model is invoked once the required time step or time is achieved. The debonding at bolt–grout interface and the plastic hinge of the rockbolt could also be simulated using this model. The force restraints of rockbolts will add at the end of the multi-time step procedure (after point G, as shown in Fig. 1). The rockbolt performances are monitored for data output purposes.

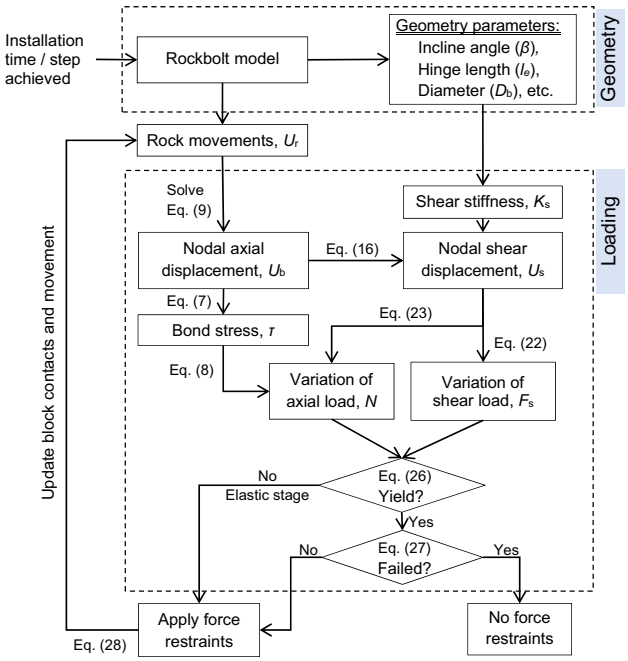

Fig. 7 Flowchart to integrate the rockbolt model into DDA

3 Verification of the DDA-Based Rockbolt Model

3.1 Comparison with Single Shear Test

To verify the accuracy of the proposed rockbolt model, DDA simulations are carried out to simulate the laboratory tests conducted by Chen and Li (2015). Two blocks with width of 0.95 m and length of 1.0 m are used in the DDA model, see Fig. 8a. The co-edge of the two blocks is set as a frictionless joint with no cohesion and tensile strength. The bottom edge of the lower block is fixed in the horizontal and vertical directions, while the top edge of the upper block can only move horizontally. The rockbolts with diameter

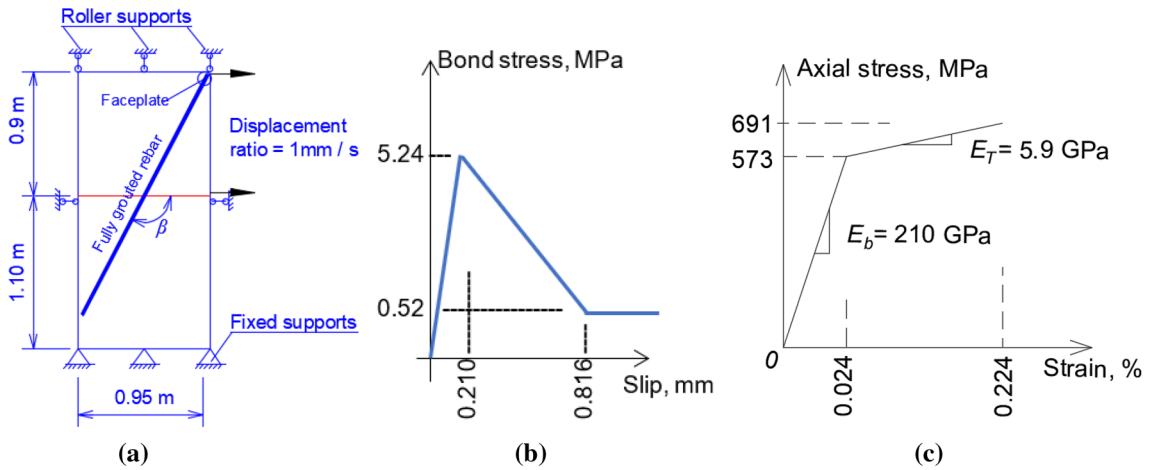

Fig. 8 Modelling the rockbolt shear test conducted by Chen and Li (2015) **a** numerical model, **b** trilinear bond-slip model at interface and **c** bilinear constitutive model of rockbolt material

of $D_b = 20$ mm are installed in the rock block with incline angle of β. The length of the rockbolt element is set as 0.1 m in rock block, except the rockbolt element crossing the joint which is assumed with a length of $4D_b$ where D_b is the diameter of rockbolt element. The end of the rockbolt where the faceplate is attached is fixed onto the block, while the other end is free to move along the rockbolt direction. The bonding behavior between the rockbolt and the two rock blocks is simulated using the trilinear model, as shown in Fig. 8b. The rockbolt is assumed as a bilinear strain-hardening steel bar based on the pullout tests results of the fully grouted rebar. The rockbolt has elastic modulus of $E_b = 210$ GPa and strain-hardening modulus of $E_T = 5.9$ GPa, see Fig. 8c. More details of the materials' properties and DDA settings are summarized in Table 1.

The DDA simulations of the pullout test and the shear tests are carried out to investigate the performance of the fully grouted rockbolts installed with incline angle $\beta = 90°$, 120°, and 140°. The stress statuses of the rockbolt at failure are shown in Fig. 9. It can be found that all the three rockbolts failed at the joint between the two blocks. The total force, defined as $F_t = \sqrt{N^2 + F_s^2}$ (Chen and Li 2015), versus total displacement curves are shown in Fig. 10. Reasonable agreement could be observed between the simulation and the laboratory tests results. The total forces of the rockbolts at yielding and at failure under shearing are significantly lower than those under pure tension (i.e., pulling out loads). The bearing capacity of the rockbolts varies with the change of the incline angles. The bearing capacity decreases for the incline angle ranging from 90° to 140°. The curves for the total forces versus displacements obtained from the DDA simulations have steeper gradients than those from the laboratory shear tests. One possible reason for the gradient difference is that the mortar deformations in the laboratory tests are not considered in the current rockbolt models. However, the yield loads from the laboratory shear tests match with those from DDA simulations with maximum difference of only 5% as shown in Table 2. For the ultimate load under shearing, the maximum difference is 23.95% for the case with the incline angle $\beta = 90°$. It should be noted that the DDA simulation could not present the dip in the total forces during failure which is caused by the assumed bi-linear material model. The difference between the DDA simulation and the yield load from the laboratory test is less than 1.0% for the pullout test, while the difference is only 0.7% for the ultimate load.

Table 1 Parameter setting in the DDA model

Item	Parameter	Values
Rock	Elastic modulus E_r, GPa	30
	Poisson ratio, v	0.2
	Unit weight, $\times 10^3$ kN/m^3	26.0
DDA calculation	Maximum displacement ratio	0.0004
	Upper limit of time interval	0.0002
	SOR factor	1.4
Rockbolt	Diameter D_b, mm	20
	Elastic modulus E_b, GPa	210
	Yield axial strength, kN	180
	Ultimate axial strength, kN	217
	Hinge length l_e, mm	40 (~$2.0D_b$)
	Shear stiffness K_s, MN/m	67.3

3.2 Comparison with Double Shear Test

The proposed fully grouted rockbolt model is used to simulate the double shear tests conducted by Forbes et al. (2017). In their laboratory tests, an optical strain sensing technique

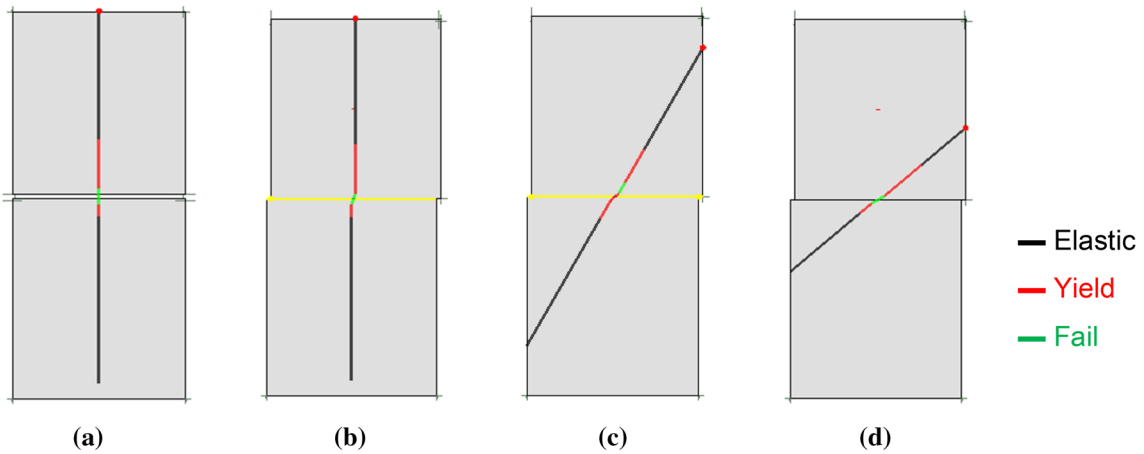

Fig. 9 Stress status of the rockbolts installed in rock blocks under **a** pull-out load, and shear load for rockbolt installed with inclined angles of **b** $\beta = 90°$, **c** $\beta = 120°$ and **d** $\beta = 140°$

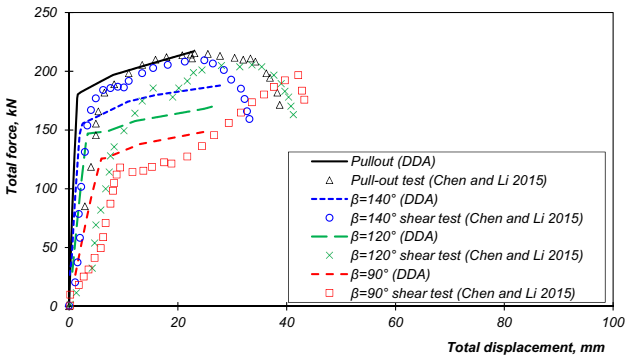

Fig. 10 Comparison of the load-deformation curves from the DDA simulations and the laboratory tests conducted by Chen and Li (2015)

Table 2 Comparison between the DDA model and the laboratory tests conducted by Chen and Li (2015)

Items	A. Pull out	B. $\beta=90°$	C. $\beta=120°$	D. $\beta=140°$
Yield axial load, kN				
Laboratory	181.86	118.13	149.45	165.92
DDA	180.05	114.93	146.64	157.60
Difference	− 1.0%	− 2.7%	− 1.9%	− 5.0%
Ultimate axial load, kN				
Laboratory	215.38	196.70	205.49	209.34
DDA	216.97	149.66	169.63	185.07
Difference	0.7%	− 23.9%	− 17.5%	− 11.6%

was developed to monitor the strain profile of fully grouted rock bolts with a spatial resolution of 0.65 mm. The single optical fibre sensor within three 2 × 2 mm machined out grooves were extended the entirety of the bolt length to measure the strain profile during the double shear tests. Three blocks with dimensions of 400 × 400 mm are used to simulate the double-jointed apparatus, as shown in Fig. 11. The rock blocks at the two sides of the model are restrained by vertical rollers. A fully grouted rockbolt with a diameter of 20 mm and a length of 1.2 m is installed in the centre of three blocks. Both ends of the fully grouted rockbolt are free to move. During the shearing process, the middle block moves downwards at a constant speed of 0.5 mm/min. The properties of the material are the same as those listed in Table 1.

Figure 12a presents the load distributions along the fully grouted rockbolt when the middle block moves 2 mm downwards. As the grooving process of the sensing may decrease the strength and rigidity of rockbolt (Forbes et al. 2017), only the shape of the axial strain distribution is given in the laboratory test. It can be seen that the DDA simulated axial load distribution is able to fit the shape of axial strain obtained by the laboratory test. Due to the shear component of the load at joint, the total load is increasing in the rockbolt element crossing the rock joint. Yielding occurs in the rockbolt elements which are near the two rock joints under such a displacement. The rockbolt nodes in the middle rock block and the first three nodes near the rock joints in the side blocks are falling in the 2nd stage of bond-slip model. It presents the initiation of failure is located within the region of the joints. As shown in Fig. 12b, the simulated nodal transverse displacement of the fully grouted rockbolt is also compared with the lateral deflection from the experiments for the applied displacement of 2 mm and 4 mm. A good agreement between the DDA simulations and the experimental results is achieved when the applied displacement is 2 mm. However, a larger difference for the case of applied displacement of 4 mm is observed, which may be due to the limitations of the current DDA model that it cannot consider the deformation of mortar filled in the borehole.

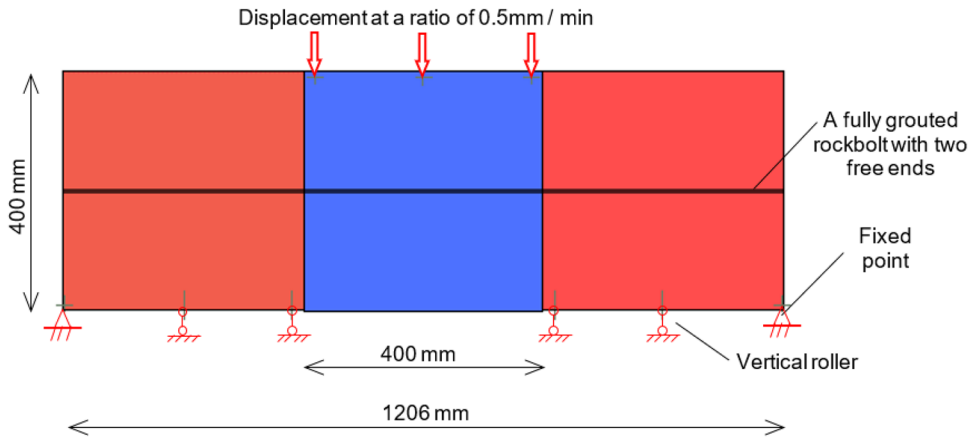

Fig. 11 DDA model of the double shear test conducted by Forbes et al. (2017)

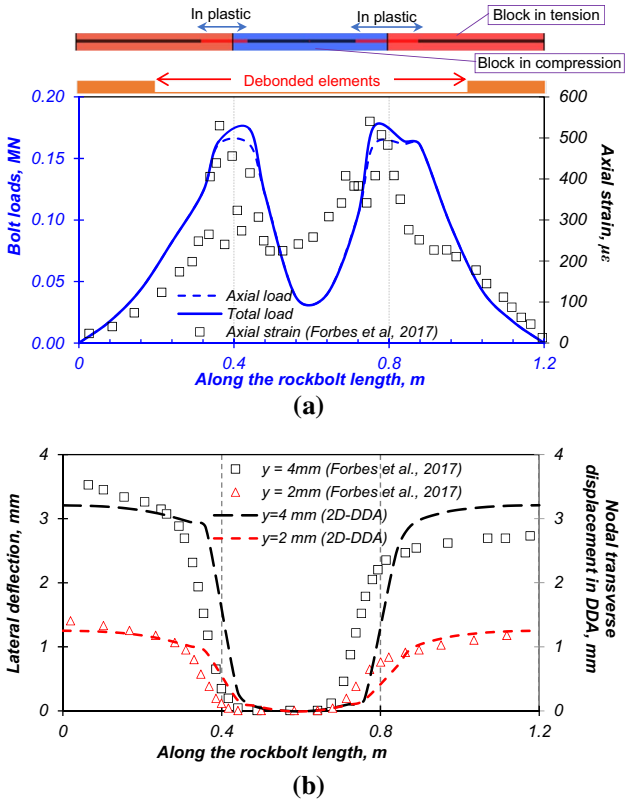

Fig. 12 Comparison of the results from the DDA simulation and the laboratory tests conducted by Forbes et al. (2017) **a** load distribution along rockbolt at applied displacement of 2 mm and **b** lateral deflection along the fully grouted rockbolt at different applied displacements

4 Conclusions

A fully grouted rockbolt model is developed and implemented into the discontinuous deformation analysis (DDA) code to study its reinforcement effort on the jointed rock masses. The analytical solutions proposed by Li et al. (2015) are used to determine the tension and shear loads of the rockbolt installed through a rock joint. The DDA-based rockbolt model is evaluated by the single shear tests conducted by Chen and Li (2015) and the double shear tests conducted by Forbes et al. (2017). The DDA simulations of the shear tests show that the proposed rockbolt model can capture the load variation during pulling and shearing procedures. The load carrying capacities during shearing decrease when the incline angle changes from 140° to 90°. The proposed DDA model could be used to present the plastic hinge formation and failure analysis for rockbolts installed in the jointed rock mass. One limitation of the proposed model is that it cannot consider the deformation of mortar filled in the borehole.

Acknowledgements This work was supported by State Key Laboratory for GeoMechanics and Deep Underground Engineering (No. SKLGDUEK1819), and the National Natural Science Foundation of China (No. 51878446).

Compliance with Ethical Standards

Conflict of interest The authors declare that they have no known conflict of interest.

References

Bahrani N, Hadjigeorgiou J (2017) Explicit reinforcement models for fully-grouted rebar rock bolts. J Rock Mech Geotech Eng 9:267–280. https://doi.org/10.1016/j.jrmge.2016.07.006

Blanco Martín L, Tijani M, Hadj-Hassen F, Noiret A (2013) Assessment of the bolt-grout interface behaviour of fully grouted rockbolts from laboratory experiments under axial loads. Int J Rock Mech Min Sci 63:50–61. https://doi.org/10.1016/j.ijrmms.2013.06.007

Bobet A, Einstein HH (2011) Tunnel reinforcement with rockbolts. Tunn Undergr Space Technol 26:100–123. https://doi.org/10.1016/j.tust.2010.06.006

Chen Y, Li CC (2015) Performance of fully encapsulated rebar bolts and D-bolts under combined pull-and-shear loading. Tunn Undergr Space Technol 45:99–106. https://doi.org/10.1016/j.tust.2014.09.008

Farmer IW (1975) Stress distribution along a resin grouted rock anchor. Int J Rock Mech Min Sci Geomech Abstr 13:A8. https://doi.org/10.1016/0148-9062(76)90297-7

Ferrero AM (1995) The shear strength of reinforced rock joints. Int J Rock Mech Min Sci Geomech Abstr 32:595–605. https://doi.org/10.1016/0148-9062(95)00002-X

Forbes B, Vlachopoulos N, Hyett AJ, Diederichs MS (2017) A new optical sensing technique for monitoring shear of rock bolts. Tunn Undergr Space Technol 66:34–46. https://doi.org/10.1016/j.tust.2017.03.007

Gerdeen JC, Snyder VW, Viegelahn GLUO (1981) Design criteria for roof bolting plans using fully resin-grouted nontensioned bolts to reinforce bedded mine roof. Volume 5. Synthesis and design criteria: 46(5)-80, 22 July 1977, 129P. Int J Rock Mech Min Sci Geomech Abstr 18:38. https://doi.org/10.1016/0148-9062(81)90937-2

Grasselli G (2005) 3D Behaviour of bolted rock joints: experimental and numerical study. Int J Rock Mech Min Sci 42:13–24. https://doi.org/10.1016/j.ijrmms.2004.06.003

Hatzor Y, Ma G, Shi G (2017) Discontinuous deformation analysis in rock mechanics practice. CRC Press/Balkema, Leiden

Hyett AJ, Bawden WF, Reichert RD (1992) The effect of rock mass confinement on the bond strength of fully grouted cable bolts. Int J Rock Mech Min Sci Geomech Abstr 29:503–524. https://doi.org/10.1016/0148-9062(92)92634-O

Jalalifar H, Aziz N (2010) Experimental and 3D numerical simulation of reinforced shear joints. Rock Mech Rock Eng 43:95–103. https://doi.org/10.1007/s00603-009-0031-7

Karampinos E, Hadjigeorgiou J, Hazzard J, Turcotte P (2015) Discrete element modelling of the buckling phenomenon in deep hard rock mines. Int J Rock Mech Min Sci 80:346–356. https://doi.org/10.1016/j.ijrmms.2015.10.007

Li CC (2010) Field observations of rock bolts in high stress rock masses. Rock Mech Rock Eng 43:491–496. https://doi.org/10.1007/s00603-009-0067-8

Li C, Stillborg B (1999) Analytical models for rock bolts. Int J Rock Mech Min Sci 36:1013–1029. https://doi.org/10.1016/S1365-1609(99)00064-7

Li X, Nemcik J, Mirzaghorbanali A, Aziz N, Rasekh H (2015) Analytical model of shear behaviour of a fully grouted cable bolt subjected to shearing. Int J Rock Mech Min Sci 80:31–39. https://doi.org/10.1016/j.ijrmms.2015.09.005

Li L, Hagan P, Saydam S, Hebblewhite B, Li Y (2016) Parametric study of rockbolt shear behaviour by double shear test. Rock Mech Rock Eng 49:4787–4797. https://doi.org/10.1007/s00603-016-1063-4

Ma S, Nemcik J, Aziz N, Zhang Z (2014) Analytical model for rock bolts reaching free end slip. Constr Build Mater 57:30–37. https://doi.org/10.1016/j.conbuildmat.2014.01.057

Ma S, Zhao Z, Nie W, Zhu X (2017) An analytical model for fully grouted rockbolts with consideration of the pre- and post-yielding behavior. Rock Mech Rock Eng 50:3019–3028. https://doi.org/10.1007/s00603-017-1272-5

Ma S, Zhao Z, Peng J, Gui Y (2018) Analytical modeling of shear behaviors of rockbolts perpendicular to joints. Constr Build Mater 175:286–295. https://doi.org/10.1016/j.conbuildmat.2018.04.175

Nemcik J, Ma S, Aziz N, Ren T, Geng X (2014) Numerical modelling of failure propagation in fully grouted rock bolts subjected to tensile load. Int J Rock Mech Min Sci 71:293–300. https://doi.org/10.1016/j.ijrmms.2014.07.007

Nie W (2019) Reinforcement mechanism of rockbolt system for underground excavation. Ph.D., Nanyang Technological University, Singapore. https://doi.org/10.32657/10220/49777

Nie W, Zhao ZY, Ning YJ, Guo W (2014a) Numerical studies on rockbolts mechanism using 2D discontinuous deformation analysis. Tunn Undergr Space Technol 41:223–233. https://doi.org/10.1016/j.tust.2014.01.001

Nie W, Zhao ZY, Ning YJ, Sun JP (2014b) Development of rock bolt elements in two-dimensional discontinuous deformation analysis. Rock Mech Rock Eng 47:2157–2170. https://doi.org/10.1007/s00603-013-0525-1

Nie W, Zhao ZY, Guo W, Shang J, Wu C (2019) Bond-slip modeling of a CMC rockbolt element using 2D-DDA method. Tunn Undergr Space Technol 85:340–353. https://doi.org/10.1016/j.tust.2018.12.025

Pellet F, Egger P (1996) Analytical model for the mechanical behaviour of bolted rock joints subjected to shearing. Rock Mech Rock Eng 29:73–97. https://doi.org/10.1007/BF01079755

Qian Q, Zhou X (2018) Failure behaviors and rock deformation during excavation of underground cavern group for Jinping I hydropower station. Rock Mech Rock Eng 51:2639–2651. https://doi.org/10.1007/s00603-018-1518-x

Shi G (1988) Discontinuous deformation analysis: a new numerical model for the statics and dynamics of block systems. Ph.D., University of California, Berkeley

Ssj M (1996) Plastic methods for steel and concrete structures. Palgrave, London